Antispiral Waves as Sources in Oscillatory Reaction−Diffusion Media†

Ernesto M. Nicola,‡,§,|| Lutz Brusch,‡,⊥ and Markus Bär*,‡

Max-Planck-Institut für Physik komplexer Systeme, Nöthnitzer Strasse 38, D-01187 Dresden, Germany, Departament E.C.M., Facultat de Física, Universitat de Barcelona, Av. Diagonal 647, E-08028 Barcelona, Spain, Institut für Theoretische Physik, Technische Universität Berlin, PN 7-1, Hardenbergstrasse 36, D-10623 Berlin, Germany, and Centre de Bioingénierie Gilbert Durand INSA-DGBA, Avenue de Rangueil 135, F-31077 Toulouse Cedex 4, France

Received: February 20, 2004; In Final Form: May 25, 2004

Spiral and antispiral waves are studied numerically in two examples of oscillatory reaction−diffusion media and analytically in the corresponding complex Ginzburg−Landau equation (CGLE). We argue that both these structures are sources of waves in oscillatory media, which are distinguished only by the sign of the phase velocity of the emitted waves. Using known analytical results in the CGLE, we obtain a criterion for the CGLE coefficients that predicts whether antispirals or spirals will occur in the corresponding reaction−diffusion systems. We apply this criterion to the FitzHugh−Nagumo and Brusselator models by deriving the CGLE near the Hopf bifurcations of the respective equations. Numerical simulations of the full reaction−diffusion equations confirm the validity of our simple criterion near the onset of oscillations. They also reveal that antispirals often occur near the onset and turn into spirals further away from it. The transition from antispirals to spirals is characterized by a divergence in the wavelength. A tentative interpretation of recent experimental observations of antispiral waves in the Belousov−Zhabotinsky reaction in a microemulsion is given.

I. Introduction

Chemical pattern formation results typically from the interplay of reaction and diffusion and occurs in many reactions in solutions and gels[1] and in heterogeneous catalysis.[2] Reaction−diffusion (RD) processes are also believed to be at the heart of morphogenesis in biological systems.[3,4]

Rotating spiral waves are probably the most typical structures investigated so far in RD systems. They have been found initially in the Belousov−Zhabotinsky reaction[5] (a related pattern, the so-called target waves, were also found in this reaction earlier[6]). Since then, rotating spirals have been frequently observed in a variety of experimental setups including aggregation of slime molds,[7] catalytic CO oxidation,[8] cardiac tissue,[9] intracellular calcium dynamics in frog eggs,[10] and glycolytic activity in extracts of yeast cells.[11]

Spirals that organize the surrounding medium by regular emission of waves are well established under both oscillatory and excitable conditions. If several spirals populate the system then the waves emitted by neighboring spirals annihilate each other at the boundary of the spirals's spatial domains. Such boundaries constitute wave sinks. Intuition tell us that these passive objects (where waves arrive and die) do not influence the medium beyond their closest surrounding.

Recently, Vanag and Epstein reported on experiments of the oscillatory Belousov−Zhabotinsky reaction in an Aerosol OT microemulsion (BZ-AOT).[12] In their quasi two-dimensional system chemical concentration patterns are arranged as so-called "antispirals" or "antitargets". Typical snapshots of the system display closely packed domains each containing a single antispiral. As time progresses the concentration waves propagate *toward* the center of the respective antispiral. Such inward propagation seemingly contradicts our intuition of spiral cores as wave sources. A word of caution toward the terminology of spirals and antispirals is in place here: spirals and antispirals are not structures that can appear simultaneously for given parameters. Instead, they occur in different complementary regions of the parameter space. The terminology of antispirals used here is rather recent and occurs only after the cited experimental paper, which is more careful and talks of inwardly rotating spiral waves. It should also be stressed that many authors have found (what is now often called) antispirals or antitargets in numerical simulations in continuous and discrete oscillatory and chaotic media and simply classified them as spirals or targets; see, e.g., refs 13−19. More recent reports have adapted the new name antispiral in the sense it is used here.[20,21] The distinction achieved here by the prefix "anti" is sometimes also referred to as positive dispersion (spiral) and negative dispersion (antispiral).[19]

Since the phenomena of antispirals and antitargets occur frequently in the complex Ginzburg−Landau equation,[22] they should be generic in oscillatory media near onset. What comes as a surprise is rather that over so many years only spirals have been observed in experiments and the first report of an antispiral occurred only very recently.[12] This experiment led to a discussion about the "mechanism" of antispirals. Vanag and Epstein suggested that the phenomenon may be related to a Hopf bifurcation with finite wavenumber (wave bifurcation) in a extended Oregonator model, where they find group and phase velocities with opposite signs. Simulations and experiments show also "packet waves", which are wave groups that move

† Part of the special issue "Gerhard Ertl Festschrift".

* Corresponding author. E-mail: baer@mpipks-dresden.mpg.de.
‡ Max-Planck-Institut für Physik komplexer Systeme.
§ Universitat de Barcelona.
|| Technische Universität Berlin.
⊥ Centre de Bioingénierie Gilbert Durand INSA-DGBA.

10.1021/jp049213r CCC: $27.50
Published on Web 09/16/2004

in the opposite direction to the motion of the constituting waves.[23] While this argument seems valid for the quasi one-dimensional packet waves, it does, in our opinion, not apply to the two-dimensional case under consideration. After all, near a wave bifurcation in a two-dimensional medium, one typically observes traveling or standing stripes or hexagons and not spiral waves. Earlier on, Nicola et al. have reported related wave groups near a Turing-wave bifurcation and named them "drifting pattern domains".[24]

Gong and Christini have recently investigated the CGLE and prototypical two-component RD models and conjectured that antispirals only occur near the onset of oscillations.[25] We will provide further evidence for their claim. They also suggest an analytical argument and criterion for the appearance of antispirals in the CGLE coefficients. Recently, we have shown that the criterion for the occurrence of antispirals in RD models has to be modified and that antispirals in the corresponding CGLE may turn out to be spirals in the original RD model.[26] Here we present the complete analytical derivation of the differing criteria for antispirals in the CGLE and in the corresponding RD models.

When studying dynamical phenomena in RD models near the onset of pattern formation, the analysis of the corresponding amplitude equation can be instructive.[27−29] The CGLE is the amplitude equation that describes the dynamics of patterns near the onset of a supercritical Hopf bifurcation.[22] The CGLE for arbitrary RD systems is obtained following exact transformation rules.[16,30] Here, we validate our criterion for antispirals in RD systems for two simple RD systems: the FitzHugh−Nagumo and Brusselator models. We derive the CGLE coefficients for these models, apply our criterion for antispirals, and compare the result to direct numerical simulations near the Hopf bifurcation. In the CGLE, domains of the parameter space can be classified according to the relative directions (signs) of phase and group velocities in rotating waves (spirals or antispirals) in line with arguments first used by Y. Kuramoto and T. Tsuzuki to analyze wave sources of the Kuramoto−Sivashinsky equation.[31] Boundaries of the parameter domains are given by zero phase or group velocities which yield analytical criteria. Extensive numerical simulations of both RD models analyzed here corroborate this criterion's prediction near the onset of oscillations and extend it when the model's parameters are driven away form threshold. The simulations also suggest that antispirals typically disappear far away from the onset of oscillations.

This paper is organized as follows: In the next section, we will discuss theoretically the distinction between spirals and antispirals within the CGLE framework and analytically derive the criterion for either occurrence in RD models near the onset of oscillations. In the third section, we explore spirals and antispirals in two RD models near and far from the onset of oscillations. We will end this paper with a short summary and discussion of the main results.

II. Weakly Nonlinear Theory of Spirals and Antispirals

A. Reaction−Diffusion systems near a Oscillatory Bifurcation. A general RD system in two dimensions may be described by the partial differential equation

$$\partial_{\tilde{t}}\boldsymbol{u} = \boldsymbol{f}(\boldsymbol{u}, \mu) + \mathscr{D}\nabla^2\boldsymbol{u} \tag{1}$$

where $\boldsymbol{u}(\tilde{\boldsymbol{x}}, \tilde{t})$ is a vector of space- and time-dependent concentrations, $\boldsymbol{f}$ is a nonlinear vectorial function, $\mathscr{D}$ is a diffusion tensor, and μ is a control parameter. Realistic models of chemical pattern forming systems have been proposed in this form, including recent models of the BZ-AOT system by Vanag et al.[32,23] and Yang et al.[33] These include many reaction species, respectively, components of $\boldsymbol{u}$, and complex reaction terms $\boldsymbol{f}$. However, in this paper we will study simple models, namely the Brusselator[34] and the FitzHugh−Nagumo[35] models.

The vector of concentrations $\boldsymbol{u}$ of a RD system near a supercritical Hopf bifurcation with frequency Ω and eigenvector $\boldsymbol{u}_1$, can be decomposed as

$$\boldsymbol{u}(\tilde{\boldsymbol{x}}, \tilde{t}) = \boldsymbol{u}_0 + \boldsymbol{u}_1\tilde{A}(\boldsymbol{x}, t)e^{i\Omega\tilde{t}} + \boldsymbol{u}_1^*\tilde{A}^*(\boldsymbol{x}, t)e^{-i\Omega\tilde{t}} \tag{2}$$

where $\boldsymbol{u}_0$ is the stationary solution that loses stability at the bifurcation onset. The evolution of modulations $\tilde{A}(\boldsymbol{x}, t) = \sqrt{\epsilon}A(\boldsymbol{x},t)e^{ic_0t}$ of the homogeneous oscillation is described by the CGLE[28]

$$\partial_t A = A + (1 + ic_1)\Delta A - (1 - ic_3)|A|^2A \tag{3}$$

where $\epsilon = (\mu - \mu_c)/\mu_c$ measures the distance from the threshold μ_c, c_1 (c_3) gives the linear (nonlinear) dispersion, and c_0 is an overall linear frequency shift. The coordinates $\boldsymbol{x} = \sqrt{\epsilon}\tilde{\boldsymbol{x}}/\xi$ and $t = \epsilon\tilde{t}/\tau$ of the CGLE are defined by characteristic spatial and temporal scales ξ, τ and describe slow modulations in space and time. Note that intrinsic CGLE frequencies ω result only in a small correction of order $\epsilon\omega$ to the original frequency of the system at the Hopf bifurcation threshold. In the following, variables with (without) a tilde will be used in the original RD system (the derived CGLE).

Numerical simulations of the CGLE (3) in a two-dimensional system with zero flux boundary conditions provide examples of antispiral waves as shown in Figure 1.

B. Spirals and Antispirals in the CGLE. Rotating (anti)-spiral waves in the two-dimensional CGLE have the form[36]

$$A(r,\theta, t) = F(r)e^{i(\sigma\theta + f(r,t))} \tag{4}$$

in polar coordinates (r,θ). The asymptotic behavior for $r \to 0$ is $\partial f(r, t)/\partial r \sim r$, $F(r) \sim r$, and denotes a topological defect $|A| = 0$ of charge σ in the spiral core. We will focus on one-armed spiral waves with $\sigma = +1$ (-1) which are related by mirror symmetry and rotate clockwise (counterclockwise). Other authors term these solutions spiral and antispiral[37] (we will not adopt this terminology here). In this paper, both left-handed or right-handed structures can be spirals (outward propagation of phase waves) or antispirals (inward propagation of phase waves) depending on parameters.

Asymptotically for $r \to \infty$ these phase waves are characterized by $F(r) \sim \sqrt{1-q_s^2}$ and $f(r, t) \sim q_s r - \omega_s(q_s)t$ with a selected wavenumber q_s and the corresponding frequency $\omega_s(q_s) = -c_3 + q_s^2(c_1 + c_3)$. The selected wavenumber q_s is a function of the parameters c_1 and c_3 given by the nonlinear eigenvalue problem resulting form inserting eq 4 into the CGLE (3).[36]

The asymptotic wave field $f(r, t)$ may be rewritten as $q_s(r - v_{ph}t)$ with the phase velocity $v_{ph} = \omega_s/q_s$. The propagation of small perturbations of the wave is described by the group velocity $v_{gr} = \partial\omega_s/\partial q_s = 2q_s(c_1 + c_3)$. Note that since we are defining the group velocity in the radial direction, a positive value of this means that any small perturbation of the (anti)-spiral is pushed away from the core region (see, e.g., Figure 1, parts b and c). In this case the (anti)spiral acts as a source that organizes the surrounding pattern. Phase and group velocity do not necessarily point into the same direction. The phase waves move outward (inward) for positive (negative) phase velocity

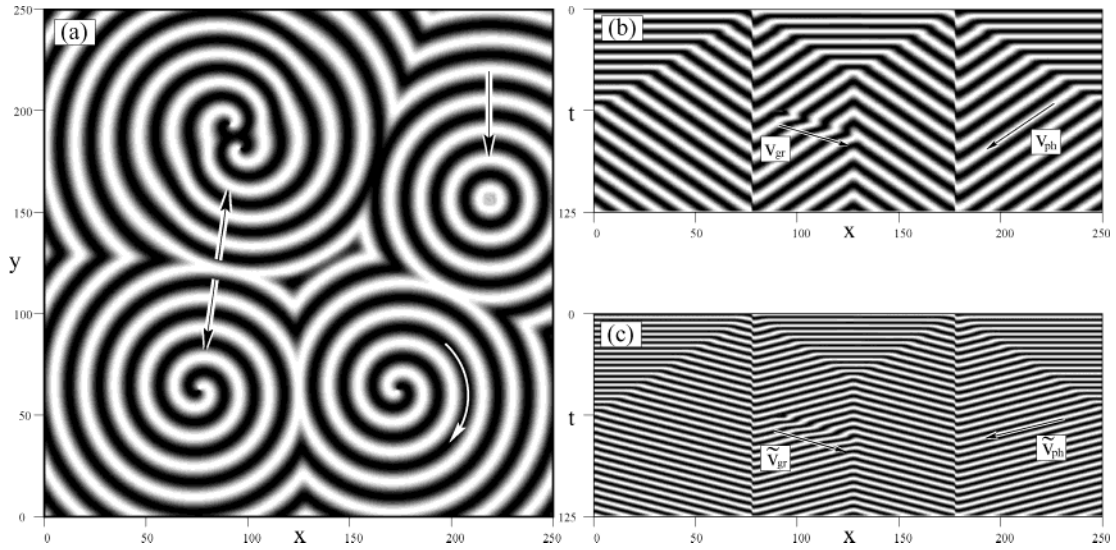

Figure 1. Numerical simulation of the CGLE (3) revealing antispirals and antitargets for $c_1 = 1$, $c_3 = 0.5$. In part a we show the real part of A in a system of size 250×250 with zero flux boundary conditions, after a transient of $t = 125$. White (black) areas correspond to maximum (minimum) values. The black arrows indicate the direction of propagation of phase waves and the white arrow denotes the rotation of an individual spiral. The inwardly propagating target waves are induced by a small oscillating heterogeneity in their center. The domain boundaries, where new waves emerge and split, are visible between the antispirals. In part b, a space-time plot of Re[A], along a horizontal cut at $y = 60$ (this line contains the cores of the antispirals at $x = 75$ and 175), is shown. After a transient of $t = 125$, the final state leads to the configuration shown in part a. Initially the cores are placed in the homogeneously oscillating background. This homogeneous background is suppressed as the antispirals grow until the whole system is filled by the antispirals at $t = 60$. Note how new waves emerge and split at the domain boundary at $x = 125$. The evolution of a small perturbation in part b illustrates the different sign of the phase and group velocities v_{ph} and v_{gr} (the artificial perturbation is applied at $x = 90$, $t = 65$ and propagates with v_{gr}). The space-time plot shown in part c corresponds to the same situation as in part b, but a fast homogeneous oscillation with $\Omega = 0.02$ has been added to the phase of A. This illustrates the dynamics in the underlying RD system which, for the value of Ω chosen, also shows antispirals (i.e., the phase velocity $\tilde{v}_{ph}$ and the group velocity $\tilde{v}_{gr}$ have the same direction as in the CGLE).

v_{ph} in the CGLE coordinates or $\tilde{v}_{ph}$ in the RD system, respectively. Hence, the signs of the selected group and phase velocities constitute the defining quantities for the occurrence of spirals or antispirals.

In the following, we calculate the parameter dependence of the introduced velocities and focus on their signs. The selected wavenumber $q_s(c_1, c_3)$ needs to be computed numerically in general, as only its asymptotics are known analytically.[36] However, for the one-dimensional (1D) analogue of the (anti)-spiral wave (i.e. for the 1D CGLE in $[0,\infty)$ with Dirichlet boundary condition: $A(0, t) = 0$) the corresponding selected wavenumber $q_{s1}(c_1, c_3)$ is known analytically[36,38]

$$q_{s1} = -\frac{3\alpha(c_1, c_3)}{2(c_1 + c_3)} \pm \sqrt{\frac{9\alpha(c_1, c_3)^2}{4(c_1 + c_3)^2} + \frac{c_3 + 2c_1\alpha(c_1, c_3)^2}{c_1 + c_3}}, \quad \text{for } c_1 + c_3 \gtrless 0 \quad (5a)$$

where

$$\alpha(c_1, c_3) = \sqrt{\frac{3c_1(8(c_1-c_3)^2+9(1+c_1c_3)^2-4c_1c_3)^{1/2}+c_1(5-9c_1c_3)-4c_3}{4(-2c_3+9c_1^3+7c_1)}} \quad (5b)$$

The function $\alpha(c_1, c_3)$ is symmetric and $q_{s1}(c_1, c_3)$ is antisymmetric under the substitution ($c_1 \to -c_1$, $c_3 \to -c_3$). The same property holds for the two-dimensional (anti)spirals as can be deduced from the form of the nonlinear eigenvalue problem:[36]

$$q_s(c_1, c_3) = -q_s(-c_1, -c_3) \quad (6a)$$

$$q_s(c_1, c_3) = 0, \quad \text{for } c_1 + c_3 = 0 \quad (6b)$$

$$q_s(c_1, c_3) > 0, \quad \text{for } c_1 + c_3 > 0 \quad (6c)$$

$$q_s(c_1, c_3) < 0, \quad \text{for } c_1 + c_3 < 0 \quad (6d)$$

Hence, q_s takes the same sign as $c_1 + c_3$. The corresponding frequency $\omega_s(c_1, c_3)$ in the CGLE fulfils $\omega_s(c_1, c_3) = -\omega_s(-c_1, -c_3)$ as had already been noted by Paullet et al.[39]

The curve where the selected frequency ω_{s1} vanishes has been computed numerically in the (c_1, c_3) parameter space (i.e., we computed the parameters c_1 and c_3 for which $\omega_{s1}(q_{s1}(c_1, c_3)) = 0$). It turns out to be different from the diagonal $c_1 + c_3 = 0$ where $q_s = 0$. Hence, within the CGLE the parameter space, we can distinguish four different domains, as shown in Figure 2. When crossing the boundaries between these domains, the phase velocity v_{ph} in the CGLE switches sign between outward and inward. Note that the spiral wavelength and v_{ph} diverge on the diagonal and v_{ph} crosses zero where $\omega_s = 0$. In the coordinate frame of the CGLE, there are two domains with spirals and two with antispirals. This result is in agreement with that of Gong et al.[25] and additionally covers two quadrants previously not considered, where the transition curve $v_{ph} = 0$ lies. Inserting eq 6 into $v_{gr} = 2q_s(c_1 + c_3)$, one finds that the group velocities v_{gr} of both spirals and antispirals never become negative.

C. Spirals and Antispirals in RD Systems. Now we return to the initial RD system. Therein the asymptotic concentration

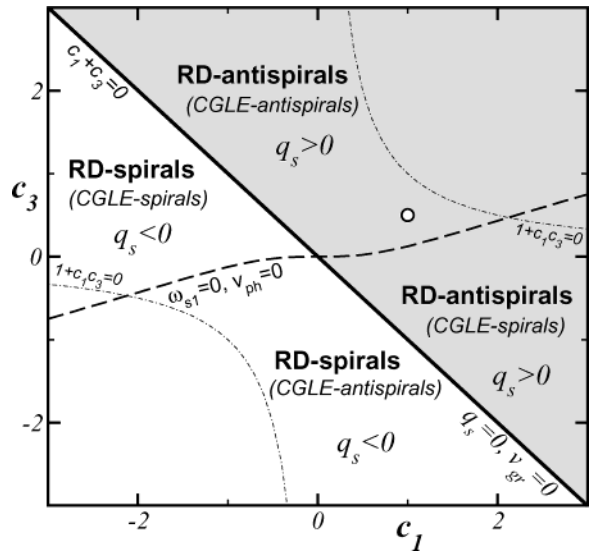

Figure 2. Parameter space (c_1, c_3) of the CGLE and domains where spiral or antispiral wave solutions exist in the CGLE and in the corresponding RD systems (where we assumed that $\Omega > 0$; see main text). The group velocity of spirals and antispirals is nonnegative everywhere. Note that in the CGLE the phase velocity vanishes along the dashed curve and antispirals (spirals) occur in the upper (lower) shaded and lower (upper) white regions. The dot−dashed curves denote the Benjamin−Feir instability ($1 + c_1c_3 = 0$). The white circle indicates the location of parameter values used in Figure 1.

waves $\boldsymbol{u} \sim e^{i\tilde{q}_s(\tilde{r}-\tilde{v}_{ph}\tilde{t})}$ with wavenumber $\tilde{q}_s = \sqrt{\epsilon}q_s/\xi$ read, after inserting eq 4 into eq 2,

$$\boldsymbol{u}(\tilde{r}, \tilde{\theta}, \tilde{t}) = \boldsymbol{u}_0 + \boldsymbol{u}_1\sqrt{\epsilon}\sqrt{1-\frac{\xi^2\tilde{q}_s^{\,2}}{\epsilon}} \times e^{i[\sigma\tilde{\theta}+\tilde{q}_s\tilde{r}-(-\Omega+\epsilon(\omega_s-c_0))\tilde{t}]} + \text{c.c.} \quad (7)$$

which yields

$$\tilde{v}_{ph} = \left[-\Omega + \frac{\epsilon}{\tau}(\omega_s - c_0)\right]/\tilde{q}_s \quad (8)$$

The description given by the CGLE (3) is accurate only if $\epsilon \ll 1$. In this limit $\tilde{v}_{ph}$ may be simplified as $\tilde{v}_{ph} \approx -\Omega/\tilde{q}_s \sim -\Omega/q_s$ (note that the same result follows for the complex conjugate (c.c.) in eq 11, where two negative signs cancel). For the group velocity we find $\tilde{v}_{gr} = v_{gr}\sqrt{\epsilon}\xi/\tau \sim v_{gr}$, which never does get negative. Therefore, both spirals and antispirals will act as organizing centers of the surrounding concentration pattern.

Let us now discuss the parameter dependence of the phase velocity $\tilde{v}_{ph} \sim -\Omega/q_s$. By convention, only the case $\Omega > 0$ is considered in the derivation of the CGLE. Then, as follows from eq 6, spirals with positive phase velocity will occur in RD systems with $c_1 + c_3 < 0$. Antispirals have $q_s > 0$ and arise in RD systems for which $c_1 + c_3 > 0$. Consequently, spirals and antispirals can never occur simultaneously within a single homogeneous system. These analytical results are summarized in Figure 2. Note finally that if the opposite sign of the primary oscillation $\Omega \rightarrow -\Omega$ is considered, then $c_1 \rightarrow -c_1$, $c_3 \rightarrow -c_3$, $\omega \rightarrow -\omega$ (as follows from complex conjugation of eq 3) and $q_s \rightarrow -q_s$ (from eq 6a), resulting in the condition $c_1 + c_3 < 0$ for the existence of antispirals in the case $\Omega < 0$.

Using eqs 8 and 6c, we compare the temporal frequencies $f = -\tilde{q}_s\tilde{v}_{ph}$ measured for a spiral (f_S) or antispiral (f_{AS}) wave with that of the homogeneous oscillation f_{bulk}

$$f_{bulk} = \Omega + \frac{\epsilon}{\tau}(c_0 + c_3) \quad (9a)$$

$$f_S = \Omega + \frac{\epsilon}{\tau}(c_0 + c_3) + \frac{\epsilon}{\tau}q_s^{\,2}|c_1 + c_3| \quad (9b)$$

$$f_{AS} = \Omega + \frac{\epsilon}{\tau}(c_0 + c_3) - \frac{\epsilon}{\tau}q_s^{\,2}|c_1 + c_3| \quad (9c)$$

We conclude $f_S > f_{bulk}$ and $f_{AS} < f_{bulk}$ in agreement with experimental observations.[12]

Let us finish this section with a short summary. The observed antispiral waves with phase velocity pointing inward were shown to be organizing centers since their group velocity points outward. Antispirals in oscillatory media therefore determine the surrounding pattern as it is the case for spiral waves. We found that a spiral in the CGLE coordinate frame may represent an antispiral in the original RD system and vice versa (see Figure 2). Altogether, in RD systems near the onset of oscillations, the antispirals are predicted to occur if the corresponding CGLE coefficients fulfil $c_1 + c_3 > 0$.

III. Reaction−Diffusion Models

To test the general predictions of the previous section we will now address our attention to a specific type RD systems. The RD systems of activator−inhibitor type are defined by[29]

$$\partial_{\tilde{t}}u = f(u, v) + \nabla^2 u \quad (10a)$$

$$\partial_{\tilde{t}}v = g(u, v) + \nabla^2 v \quad (10b)$$

where δ is the ratio of diffusion constants, and the functions $f(u, v)$ and $g(u, v)$ define the dynamics of the activator $u(\tilde{\mathbf{x}}, \tilde{t})$ and inhibitor $v(\tilde{\mathbf{x}}, \tilde{t})$, respectively.

In the following we will consider two prototypical examples of activator-inhibitor dynamics widely analyzed in the literature: the FitzHugh−Nagumo and Brusselator models. In both cases we will proceed as follows: First we will study their fixed points and analyze their linear stability. The next step will be the derivation of the coefficients c_1 and c_3 of the corresponding CGLE (3). They can be used to determine whether spirals or antispirals appear near the Hopf bifurcation. Finally we will compare these prediction with numerical simulations of both models near and far from onset.

A. FitzHugh−Nagumo Model. The FitzHugh−Nagumo (FHN) dynamics[35] is defined by[40]

$$f(u, v) = u - \frac{u^3}{3} - v \quad (11a)$$

$$g(u, v) = \epsilon(u - \gamma v + \beta) \quad (11b)$$

where $\epsilon > 0$ is the ratio between the time scales of both fields, and β and γ are parameters that determine the number of fixed points. The coordinates of these fixed points are independent of ϵ and are given by the roots of a cubic polynomial. In the following we will only consider $\gamma > 0$ and restrict our analysis to the case where a unique fixed point (u_0, v_0) exists. This is the case, for example, for $\gamma = 1/2$ where the coordinates of the fixed point are $u_0 = ((\sqrt{1+9\beta^2} - 3\beta)^{2/3} - 1)/(\sqrt{1+9\beta^2} - 3\beta)^{1/3}$ and $v_0 = (u_0 + \beta)/\gamma$.

Choosing ϵ as the control parameter and keeping β, δ, and γ constant, a linear stability analysis of (u_0, v_0) shows that it is unstable to periodic oscillations if $\epsilon < \epsilon_H^c$, where $\epsilon_H^c = (1 -$

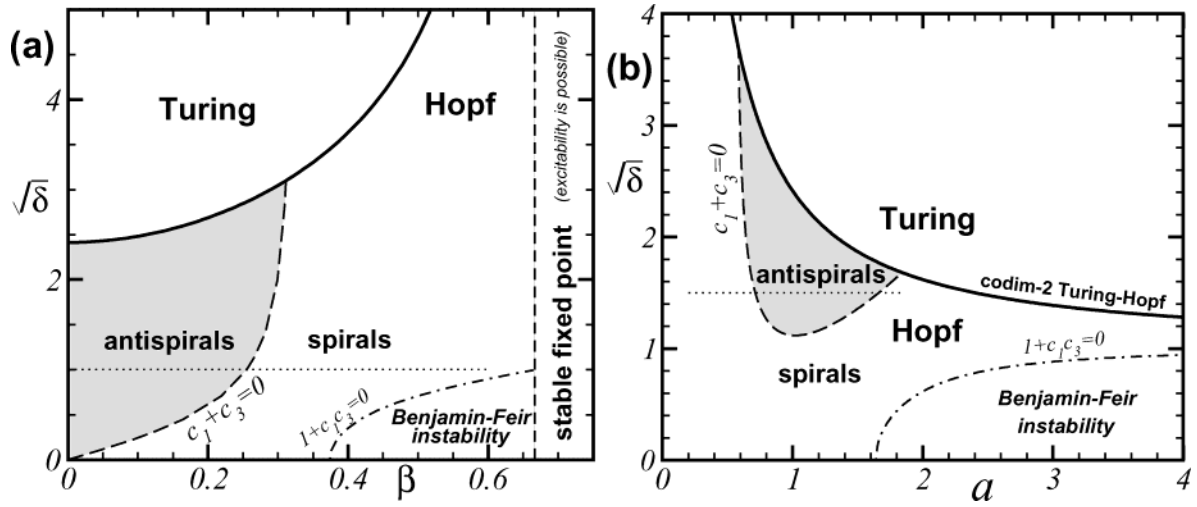

Figure 3. The gray areas show the parameter space regions where antispirals are predicted to exist near the Hopf instability threshold for the FHN and Brusselator models (in parts a and b, respectively). The thick full lines separate the regions where either the Turing or Hopf instability appears first as the control parameter ϵ (parameter b) is decreased (increased) away from threshold for the FHN model in part a (in part b, it is the Brusselator model). Inside the dot−dashed lines the Benjamin−Feir instability is predicted. The thin dotted lines indicate the range of parameter values considered in the numerical simulations of (anti)spirals summarized in Figures 4 and 6. The Hopf bifurcation considered in both figures is *supercritical* (see main text). In part a, we consider the parameter space (β, $\sqrt{\delta}$) of the FHN model (eq 11) with $\gamma = {}^1/_2$. For $\beta \geq {}^2/_3$, the fixed point (u_0, v_0) is stable and, if ϵ is small enough, excitability is possible. In part b, the control parameter (a, $\sqrt{\delta}$) of eq 12 is plotted.

$u_0^2)/\gamma$. This Hopf bifurcation has a frequency $\Omega = \sqrt{(1-u_0^2)/\gamma-(1-u_0^2)^2}$ at onset. The fixed point may also become unstable to spatially periodic perturbations with wavenumber $\tilde{q}_T = \sqrt{((1-u_0^2)\delta-\gamma\epsilon)/(2\delta)}$ (i.e., a Turing instability) if $\epsilon < \epsilon_T^c$, where $\epsilon_T^c = ((2 - (1 - u_0^2)\gamma + 2\sqrt{1-(1-u_0^2)\gamma)\delta})/\gamma^2$.

These two instabilities may occur simultaneously at a codimension-2 instability. The thick full line in Figure 3a shows the location of this codimension-2 instability in the parameter space (β, $\sqrt{\delta}$) for $\gamma = {}^1/_2$. In the following we will restrict our analysis to the Hopf instability (i.e the region below the codimension-2 line in Figure 3a).

Using the methods explained in refs 27 and 29, the derivation of the coefficients c_1 and c_3 is straightforward. Here we will only quote the main results of this derivation. The linear dispersion coefficient is given by

$$c_1 = \left(\frac{1-u_0^2}{\Omega}\right)\frac{\delta-1}{\delta+1}$$

Note that this coefficient vanishes if both fields diffuse with equal strength. If $(1 - \gamma - \gamma u_0^2)/(1 - \gamma + \gamma u_0^2) > 0$, the Hopf bifurcation is supercritical, otherwise it is subcritical and the CGLE (3) cannot be applied. For $\gamma = {}^1/_2$ (the case shown in Figure 3a) the Hopf instability is supercritical for any value of β. The result for the nonlinear dispersion coefficient c_3 is more complicated:

$$c_3 = \frac{3 - 3\gamma - 7u_0^2 + 3\gamma u_0^4}{3 - 3\gamma - 3\gamma u_0^2}\sqrt{\frac{\gamma}{(1-u_0^2)(1-\gamma+\gamma u_0^2)}}$$

We may now use the expression for the coefficients c_1 and c_3 to evaluate the conditions for the spiral−antispiral transition $c_1 + c_3 = 0$ and the Benjamin−Feir instability $1 + c_1c_3 = 0$ in the parameter space (β, $\sqrt{\delta}$). These two lines are plotted in Figure 3a. Note that the region where antispirals are predicted to occur near threshold, exists only for small values of β (i.e. far from the excitability region) and vanishes if δ is too big or if $\delta \to 0$. Moreover, for $\beta = 0$, where the model exhibits the symmetry $(u, v) \to (-u, -v)$, only antispirals are predicted.

The predicted spiral−antispiral transition at $c_1 + c_3 = 0$ is strictly valid only close to supercritical Hopf bifurcations (i.e. for $\epsilon \lesssim \epsilon_H^c$). To test this and in addition to investigate the behavior far from threshold, we have studied the FHN model numerically. We have done extensive numerical simulations of 1D-(anti)spiral analogues in eq 11 near and far from threshold. These simulations were performed in very long systems (typically including hundreds of spiral wavelengths) with the following boundary conditions: on the right side a zero flux condition is imposed and on the left side the field is kept to $u = u_0$ and $v = v_0$. The output of these numerical simulations, see Figure 4, is insensitive to initial conditions. If we wait long enough, the boundary condition in the left side (the "core") will select phase waves with a particular $\tilde{q}_{s1}$ which eventually invade the rest of the system (since they always have positive $\tilde{v}_{gr}$). Antispirals (spirals) will have negative (positive) phase velocity $\tilde{v}_{ph}$. Near the Hopf threshold, the observed behavior is equivalent to the one predicted by the CGLE. However, as ϵ is decreased, a transition from antispirals to spirals is seen. This transition is related to a change in the sign of $\tilde{q}_{s1}$ and is not captured by the CGLE description (see below).

To assess the previous results for the 1D-(anti)spiral analogue we have also carried out a number of 2D simulations of the FHN model near onset. The outcome of these simulations is shown in Figure 4b and confirms that, at least near the onset, the 1D analogue provides a good description of the spiral−antispiral transition mechanism in the 2D system. To see this more quantitatively, in Figure 5 we plot, against ϵ, the selected wavenumbers $\tilde{q}_s$, $\tilde{q}_{s1}$, in 1D and 2D, and the corresponding wavenumbers in the CGLE in 1D and 2D (using the coefficients derived in this section), for the case $\beta = 0$ and $\delta = 1$. Note, in the inset, the dramatic disagreement between the measured wavenumbers and the predicted by the CGLE as the distance to the threshold is increased. Figure 5 makes explicit the change of sign of $\tilde{q}_s$ occurring for small values of ϵ. Also note that, although the measured $\tilde{q}_s$ gets apart from $\tilde{q}_{s1}$ as the distance to onset increases, the qualitative behavior is the same.

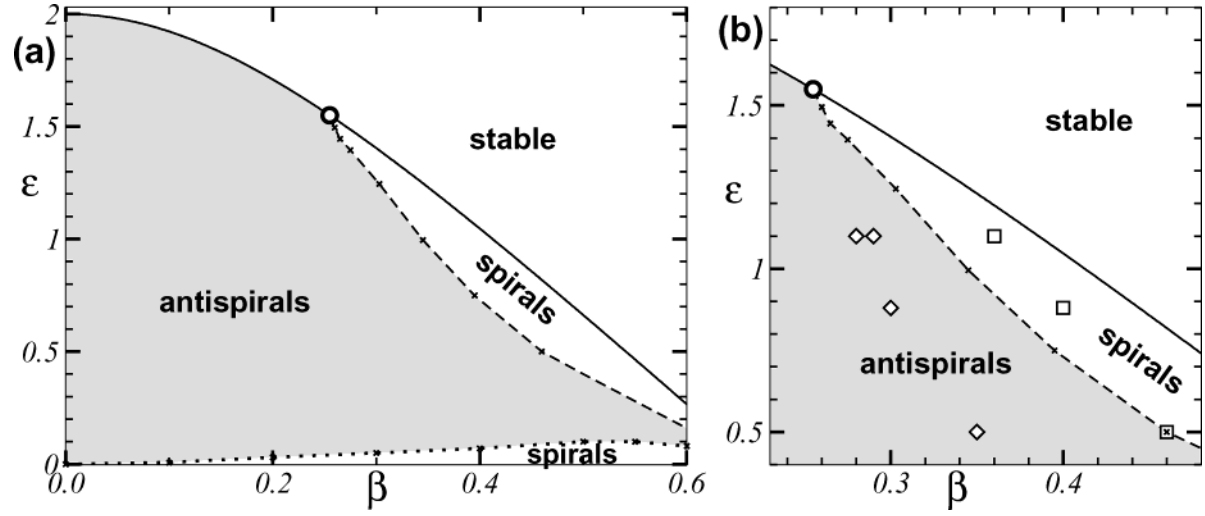

Figure 4. Summary of the results of numerical simulations of 1D- and 2D-(anti)spirals in the FHN model. The thick full line in part a indicates the location of the Hopf instability threshold. The white circle indicates the spiral−antispiral transition point at onset, as predicted by the criterion $c_1 + c_3 = 0$ (cf. Figure 3). The dashed curve indicates the spiral−antispiral transition of the 1D-(anti)spiral analogue which was computed numerically. The thick dotted line shows the antispiral−spiral transition occurring for small values of ϵ. In part b, a magnification of the region where the spiral−antispiral transition occurs near onset is shown. The squares and diamonds indicate the location of 2D numerical simulations (cf. Figure 1), resulting in spirals and antispiral, respectively. The parameters are $\sqrt{\delta} = 1$ and $\gamma = 1/2$. Refer to Figure 3 for a resume of the location of these simulations in the parameter spaces (β, $\sqrt{\delta}$).

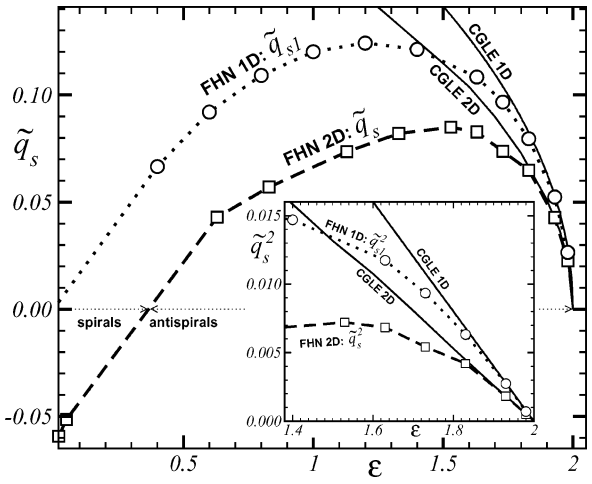

Figure 5. Plot of the measured wavenumber $\tilde{q}_s$ selected by 1D- and 2D-(anti)spirals (open circles and squares, respectively) in numerical simulations of the FHN model (11) as a function of the parameter ϵ, with $\sqrt{\delta} = 1$ and $\beta = 0$ (in this case $\gamma = 1/2$ and $\epsilon_H^c = 2$). The full lines indicate the wavenumber selected by the 2D antispirals and 1D antispiral analogues in the CGLE. The **CGLE 1D** line is calculated using the wavenumber $\tilde{q}_{s1}^2$ predicted analytically by Hagan's formula (5). In the inset the value of $\tilde{q}_S^2$ in the region close to the onset is shown. Note that the **CGLE 1D** and **CGLE 2D** lines are directly proportional to the distance to the threshold $\sqrt{\epsilon_H^c - \epsilon}$ and consequently that both q_{s1} and q_s are constant in the framework of the amplitude equations, but also note that these constant values differ.[38] The measured $\tilde{q}_{s1}$ and $\tilde{q}_s$ approach (as expected) the predictions of the 1D and 2D CGLE antispirals near the threshold but are systematically smaller far away from it.

B. Brusselator Model. Let us finally address the Brusselator dynamics.[34] This model is defined by

$$f(u, v) = a - (b + 1)u + u^2 v \tag{12a}$$

$$g(u, v) = bu - u^2 v \tag{12b}$$

where a and b are two parameters (assumed in the following to be positive). This model has a unique fixed point $(u_0, v_0) = (a, b/a)$, for any value of the parameters a, b, and δ.

Similar to the FitzHugh−Nagumo model, we may now examine the stability of the fixed point. Let us take b as the control parameter. Depending on the values of the parameters a and δ, the fixed point (u_0, v_0) may become unstable in two different ways. If $b > b_H^c$, where $b_H^c = 1 + a^2$, then a Hopf instability with frequency $\Omega = a$ occurs. In the other hand, if $b > b_T^c$, where $b_T^c = (1 + a/\sqrt{\delta})^2$, a Turing instability with wavenumber $\tilde{q}_T^2 = a/\sqrt{\delta}$ takes place. These instabilities may occur simultaneously in a codimension-2 line. This line and the regions in the parameter space $(a, \sqrt{\delta})$ where either the Hopf or Turing instabilities appear first, as the control parameter b is increased, are shown in Figure 3b.

A short calculation[27] shows that the coefficients c_1 and c_3 are

$$c_1 = a\frac{\delta - 1}{\delta + 1} \quad \text{and} \quad c_3 = \frac{7a^2 - 4 - 4a^4}{3a(2 + a^2)}$$

The spiral/antispiral transition line $c_1 + c_3 = 0$ is plotted in the parameter space $(a, \sqrt{\delta})$ in Figure 3b. Note that the region where antispirals are predicted is rather small and is located near the area where of the Turing instability appears first. Also in this case the antispirals will occur only for intermediate values of the diffusion ratio δ.

We have performed numerical simulations also for this model. As for the FHN model, we investigated 1D-spirals and antispirals (with the same boundary conditions as in the previous study). The results of these simulations are resumed in Figure 6. In this figure we also show the output of some 2D simulations, which confirm the observation that 1D simulations provide a good estimate for the location of the spiral−antispiral transition. Also here it is seen that the prediction based in the CGLE description is only valid in the vicinity of the Hopf threshold. As the distance to this threshold increases the antispirals are turned into spirals.

IV. Summary

In this paper, we emphasize the fact that the essential difference between spirals and antispirals is the sign of phase

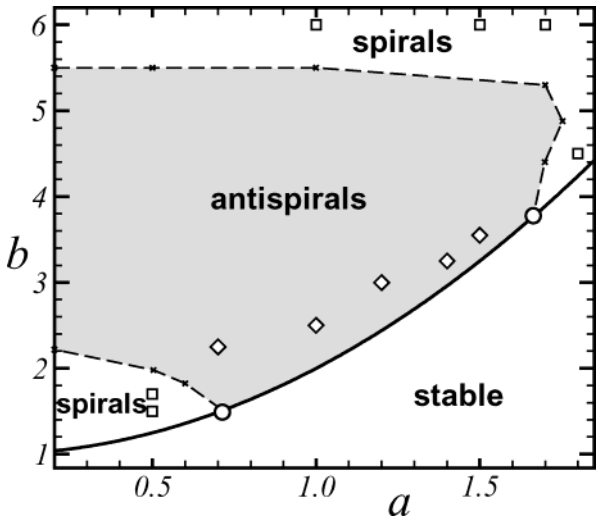

Figure 6. Summary of the results of numerical simulations of 1D- and 2D-(anti)spirals in the Brusselator model with $\sqrt{\delta} = 1.5$. The thick full line indicates the location of the Hopf instability threshold and the white circles indicate the spiral−antispiral transition points at onset (cf. Figure 3). The dashed curves indicate (approximately) the analogue of the spiral−antispiral transition in the 1D calculations. The squares and diamonds show the location of some 2D numerical simulations resulting in spirals and antispirals, respectively.

velocity of the travelling waves emanating from the core region and that phase and group velocity do not necessarily have to point into the same direction. Consequently, we may conclude that spirals and antispirals cannot occur simultaneously. They appear in different regions of the parameter space.

We have shown that spirals and antispirals are related by a simple symmetry transformation in the parameter space of the CGLE and derived a criterion for the CGLE coefficients, namely $c_1 + c_3 > 0$, that predicts the existence of antispirals in the respective RD model near a Hopf instability. In the CGLE parameter space, antispirals appear as frequently as spirals. Spirals and antispirals are found in complementary regions of the parameter space and are characterized by the selection of positive and negative wavenumbers, respectively. At the boundary between antispirals and spirals, the selected wavenumber is zero and the selected wavelength diverges. Our criterion has been mapped to the parameter space of two representative RD models. The analysis of both models suggests that to get antispirals it is necessary that the inhibitor also diffuses. Moreover, the diffusion constants of both reactants should be of similar magnitude in order to find antispirals. This is likely to occur near the codimension-2 Turing−Hopf instability. We have also performed numerical simulations of both models near and far form the oscillatory instability threshold. Antispirals are quite likely to appear near the Hopf bifurcation but turn into regular spirals far into the oscillatory where the amplitude of waves becomes large. The assumption that the 1D spiral analogue gives a good approximation of the spiral−antispiral transition behavior near onset was validated by both examples discussed in this paper. Furthermore, they suggest that this approximation still holds moderately far from the thresholds of oscillation.

In a more general distinction, antispirals emit phase waves that are typical for oscillatory media. In contrast, trigger waves common in excitable media should always have the same sign of group and phase velocity. Since the distinction between trigger and phase waves is not sharp, we cannot make a general statement about the possibility of antispirals in excitable media but expect that they will be quite hard to find therein. The rarity of experimental observations of antispirals suggests that most experiments exhibiting spirals are conducted either far away from the oscillatory threshold or under excitable, respectively, bistable conditions. It is tempting to explain the experiment of Vanag and Epstein[12] from the proximity of the control parameters to a Hopf bifurcation, though other more complicated possibilities cannot be ruled out at this stage.

Finally, we would like to stress the most essential point in the consideration of the nature of spirals and antispirals. The crucial quantity for both structures is the group velocity of the periodic waves outside the core region. In all models considered, the group velocity is pointing outward from the spiral core as has been shown analytically for the CGLE. The distinction between spirals and antispirals stems only from the sign of the phase velocities and the corresponding phenomenological impression. In our opinion, it is important not to confuse the distinction between spirals and antispirals with the distinction between sinks and sources. Several authors have pointed out that the definition of a source depends only on the group velocities and not at all on the phase velocity of the periodic waves far away from it.[41,42] Counting arguments show that sources belong typically to a zero-parameter family while sinks are members of a two parameter family.[41] In other words, sources select frequency and wavelength of the emitted periodic waves, while sinks simply appear where two wave trains of arbitrary wavelength and period happen to meet. A classification of defects in RD media can be done according to the group velocities of periodic waves on both sides of the defect and the velocity of the defect itself. Apart from sources and sinks, one may also find transmission defects (one-parameter family) and contact defects in RD media.[42] In the present context, spirals and antispirals are both sources; i.e., they select their frequency and wavelength and control their surroundings. If they were sinks (as sometimes claimed in the literature), the waves would have to be organized from the domain boundaries, which would require another unknown "organizer" structure. Altogether, we have shown by combination of existing analytical arguments that antispirals are structures of similar nature as spirals and should hence be expected in many systems exhibiting phase waves in particular near the onset of oscillations. Their experimental discovery can be nicely interpreted within the existing theoretical framework for oscillatory RD media.

Acknowledgment. We are grateful to I. Aranson, L. Kramer, H. Swinney, and V. Vanag for discussions. Financial support by the German−Israeli Foundation (GIF) is gratefully acknowledged. E.M.N. would like to express thanks for financial support given by the Sonderforschungsbereiche (SFB) 555 der DFG: "Komplexe nichtlineare Prozesse" (Berlin, Germany), by the European Commission under network HPRN-CT-2002-00312 and by DGI (Spain) under Project BQU2003-05042. L.B. acknowledges the support of the Max Planck Society through an Otto Hahn fellowship.

References and Notes

(1) *Chemical waves and patterns*; Kapral, R., Showalter, K., Eds.; Kluwer: Dordrecht, The Netherlands, 1994.

(2) Imbihl, R.; Ertl, G. *Chem. Rev.* **1995**, *95*, 697.

(3) Murray, J. *Mathematical Biology*; Springer: Berlin, 1989.

(4) Keener, J.; Sneyd, J. *Mathematical Physiology*; Springer: New York, 1998.

(5) Winfree, A. T. *Science* **1972**, *175*, 634.

(6) Zaikin, A. N.; Zhabotinsky, A. M. *Nature (London)* **1970**, *225*, 535.

(7) Gerisch, G. *Naturwissenschaften* **1971**, *58*, 430. Devreotes, P. *Science* **1989**, *245*, 1045.

(8) Jakubith, S.; Rotermund, H.-H.; Engel, W.; von Oertzen, A.; Ertl, G. *Phys. Rev. Lett.* **1990**, *65*, 3013. Nettesheim, S.; von Oertzen, A.; Rotermund, H.-H.; Ertl, G. *J. Chem. Phys.* **1993**, *98*, 9977.

(9) Davidenko, J. M.; Pertsov, A. M.; Salomonsz, R.; Baxter, W.; Jalife, J. *Nature (London)* **1991** *353*, 349.

(10) Lechleiter, J.; Girard, S.; Peralta, E.; Clapham, D. *Science* **1991**, *252*, 123.

(11) Mair, Th.; Müller, S. C. *J. Biol. Chem.* **1996**, *271*, 627.

(12) Vanag, V. K.; Epstein, I. R. *Science* **2001**, *294*, 835.

(13) Yamada, T.; Kuramoto, Y. *Prog. Theor. Phys.* **1976**, *55*, 2035.

(14) Selpuchre, J. A.; Dewel, G.; Babloyantz, A. *Phys. Lett. A* **1990**, *147*, 380.

(15) Goryachev, A.; Kapral, R. *Phys. Rev. Lett.* **1996**, *76*, 1619.

(16) Ipsen, M.; Hynne, F.; Sorensen, P. G. *Int. J. Bif. Chaos* **1997**, *7*, 1539.

(17) Tobias, S. M.; Knobloch, E. *Phys. Rev. Lett.* **1998**, *80*, 4811.

(18) Rabinovitch, A.; Gutman, M.; Aviram, I. *Phys. Rev. Lett.* **2001**, *87*, 084101.

(19) Stich, M.; Mikhailov, A. S. *Phys. Chem.* **2002**, *216*, 521.

(20) Woo, S.-J.; Lee, J.; Lee, K. J. *Phys. Rev. E* **2003**, *68*, 016208.

(21) Skødt, H.; Sørensen, P. G. *Phys. Rev. E* **2003**, *68*, 020902.

(22) Aranson, I. S.; Kramer, L. *Rev. Mod. Phys.* **2002**, *74*, 99.

(23) Vanag, V. K.; Epstein, I. R. *Phys. Rev. Lett.* **2002**, *88*, 088303.

(24) Nicola, E. M.; Wolf, W.; Or-Guil, M.; Bär, M. *Phys. Rev. E* **2002**, *65*, 055101.

(25) Gong, Y.; Christini, D. J. *Phys. Rev. Lett.* **2003**, *90*, 088302.

(26) Brusch, L.; Nicola, E. M.; Bär, M. *Phys. Rev. Lett.* **2004**, *92*, 089801.

(27) Kuramoto, Y. *Chemical Oscillations, Waves, and Turbulence*; Springer-Verlag: Berlin, 1984.

(28) Cross, M. C.; Hohenberg, P. C. *Rev. Mod. Phys.* **1993**, *65*, 851.

(29) Nicolis, G. *Introduction to Nonlinear Sciences*; Cambridge University Press: Cambridge, England, 1995.

(30) Ipsen, M.; Kramer, L.; Sørensen, P. G. *Phys. Rep.* **2000**, *337*, 193.

(31) Kuramoto, Y.; Tsuzuki, T. *Prog. Theor. Phys.* **1976**, *55*, 356.

(32) Vanag, V. K.; Epstein, I. R. *Phys. Rev. Lett.* **2001**, *87*, 228301.

(33) Yang, L.; Dolnik, M.; Zhaotinsky, A. M.; Epstein, I. R. *J. Chem. Phys.* **2002**, *117*, 7258.

(34) Prigogine, I.; Lefever, R. *J. Chem. Phys.* **1968**, *48*, 1695.

(35) FitzHugh, R. *Biophysics* **1961**, *1*, 445. Nagumo, J. S.; Arimoto, S.; Yoshizawa, S. *Proc. IRE* **1962**, *50*, 2061.

(36) Hagan, P. S. *SIAM J. Appl. Math.* **1982**, *42*, 762.

(37) Komineas, S.; Heilmann, F.; Kramer, L. *Phys. Rev. E* **2000**, *63*, 011103.

(38) Bodenschatz, E.; Weber, A.; Kramer, L. In *Nonlinear Wave Processes in Excitable Media*, Holden, A. V., Markus, M., Othmer, H. G., Eds.; Plenum Press: New York, 1990. Aranson, I. S.; Aranson, L.; Kramer, L.; Weber, A. *Phys. Rev. A* **1992**, *46*, 2992.

(39) Paullet, J.; Ermentrout, B.; Troy, W. *SIAM J. Appl. Math.* **1994**, *54*, 1386.

(40) Winfree, A. T. *Chaos* **1991**, *1*, 303.

(41) van Hecke, M.; Storm, C.; van Saarloos, W. *Physica D* **1999**, *134*, 1.

(42) Sandstede, B.; Scheel, A. *SIAM J. Appl. Dyn. Syst.* **2004**, **3**, 1.